PSILOGOS

Research Article

open-access

Trajectory-Encoded Pharmacological Recovery in Virtual Human Cortical Organoids Across Schizophrenia, Major Depressive Disorder, and Bipolar Disorder

Erik Johansson

ABSTRACT

Patient-derived neural cultures can reveal cellular abnormalities that are obscured by symptom-based psychiatric categories, yet drug-response studies commonly reduce a changing biological process to one observation time and one readout. This study asks whether the shape of a neuroimmune perturbation response can distinguish schizophrenia, major depressive disorder, and bipolar disorder while identifying the pharmacological exposure that produces the broadest cellular recovery. A biologically constrained simulation generated 120 virtual donor lines, equally divided among the three disorders and unaffected controls. Each donor contributed triplicate cortical-organoid observations under an unchallenged condition, tumor necrosis factor alpha (TNF-α) alone, or TNF-α followed by loxapine, ketamine, or lithium. Network synchrony, neurite complexity, mitochondrial membrane potential, excitation–inhibition balance, and interleukin-6 secretion were sampled at 0, 6, 24, and 72 h, yielding 7,200 records and 36,000 outcome values. Trajectory-encoded perturbation phenotyping represented every donor by interval changes and curvature terms rather than isolated values. Five-fold grouped cross-validation produced 0.700 balanced accuracy for four-class donor classification, with class-wise F1 values of 0.900, 0.585, 0.632, and 0.690 for control, schizophrenia, major depression, and bipolar disorder, respectively. Integrated recovery fractions showed disorder-selective maxima: loxapine in schizophrenia (0.506, 95% bootstrap interval 0.467–0.547), ketamine in major depression (0.499, 0.471–0.528), and lithium in bipolar disorder (0.571, 0.538–0.604). Removing interleukin-6 features reduced balanced accuracy most strongly, from 0.700 to 0.650, whereas removing excitation–inhibition features increased it to 0.758, indicating partial redundancy. These simulation findings answer the study question affirmatively within the stated generative assumptions: temporal, multireadout responses contain diagnostic and treatment-ranking information that static measurements discard. The results define falsifiable expectations for a donor-blocked organoid study and do not constitute clinical evidence.

Keywords: cerebral organoids; induced pluripotent stem cells; neuroimmune perturbation; temporal phenotyping; schizophrenia; major depressive disorder; bipolar disorder; pharmacological recovery

Department of Clinical Neuroscience, Centre for Psychiatry Research, Karolinska Institutet, Stockholm, Sweden
ejohanson23@gmail

– **Published:** 15 December 2024

1. INTRODUCTION

Psychiatric diagnosis is indispensable for communication and care, but diagnostic labels do not imply a single cellular cause. Schizophrenia, major depressive disorder (MDD), and bipolar disorder (BD) each encompass substantial variation in age at onset, symptom course, cognitive burden, comorbidity, and treatment response. Their boundaries are also biologically permeable. Genetic liability is distributed across many loci, cellular pathways recur across diagnoses, and a treatment that is effective for one subgroup can be ineffective or poorly tolerated in another. A useful preclinical assay must therefore do more than reproduce an average case. It should retain donor-to-donor variation, permit controlled perturbation, and measure whether a pharmacological intervention restores several coupled cellular functions rather than changing an isolated molecular signal.

Animal studies remain valuable for systemic pharmacology and behavior, although species differences complicate the interpretation of developmental processes that depend on human-specific transcriptional programs. Human neural development contains cell populations, temporal schedules, and cortical architectures that are not simple scaled versions of those in rodents.[24,25,37] Induced pluripotent stem cells (iPSCs) provide a complementary route because somatic cells can be returned to pluripotency and directed toward neural lineages while retaining much of the donor's genetic background.[1,38] Monolayer cultures permit controlled access to neurons and glia, but spatial organization, maturation gradients, and cell–cell interactions are restricted. Three-dimensional neural cultures partly address these limitations by allowing progenitors and differentiated cells to self-organize within a tissue-like volume.[14,23]

Cerebral organoid technology has progressed from a broad model of early brain development to preparations with region-selective identities, reproducible cortical layering, and measurable circuit activity. The early demonstration that pluripotent cells could self-organize into cerebral tissue established the feasibility of modeling developmental pathology in a human cellular setting.[26] Later work produced midbrain, brainstem, cerebellar, spinal, and cortical preparations, illustrating that protocol choice can enrich particular neuronal populations and developmental programs.[15,21,28,30] Sliced cortical organoids alleviate diffusion constraints and allow prolonged examination of cortical layer formation,[31] while forebrain assembloids permit interactions between regionally distinct populations.[5] These advances do not make an organoid equivalent to a brain, but they enlarge the range of cellular questions that can be asked with human material.

The most persistent technical limitations are variability, incomplete maturation, and restricted vascular support. Organoid size, regional identity, cell composition, and necrotic burden can differ across batches. Long culture periods amplify handling and incubator effects, while diffusion gradients make the center of a large organoid biologically different from its surface. Microfluidic perfusion and sensor-integrated culture devices offer one route to more stable exposure and repeated measurement.[20,45] These systems can control fluid exchange, reduce abrupt dosing artifacts, and monitor secreted products without destroying the tissue. Even with such improvements, donor lines, clones, differentiations, and wells must be treated as distinct levels of variation rather than pooled as independent samples. Statistical design is consequently inseparable from biological design.

Patient-derived models of schizophrenia consistently implicate early neuronal development, synaptic connectivity, mitochondrial function, and excitation–inhibition regulation. Reduced neurite extension and connectivity were observed in schizophrenia-derived neural cells, together with altered gene expression involving developmental signaling.[7,8] Mitochondrial dysfunction and impaired differentiation have also been documented, and transfer of healthy mitochondria improved neuronal differentiation in patient-derived cells.[32,33] Cerebral organoids have connected abnormal cortical development to altered fibroblast growth factor receptor signaling.[29,36] Single-cell analyses further suggest that excitation–inhibition imbalance can emerge during development and differ between genetically related individuals.[34] These findings support multireadout measurement because no single feature adequately represents the disorder.

Environmental challenge is especially relevant to a developmental assay. A genetic susceptibility may remain only partly visible under stable culture conditions and become more pronounced after inflammatory, metabolic, or pharmacological stress. Heat-shock factor 1 links fetal environmental stress to neuronal vulnerability.[18] Exposure to TNF-α disrupts organoid development and produces a larger effect in schizophrenia-derived tissue than in control tissue.[4] Such observations motivate a perturb-and-recover design: the challenge probes reserve capacity, and treatment is evaluated by the extent and timing of recovery. A static comparison at one time can miss the depth of injury, delay of response, or later rebound.

MDD supplies a different but overlapping set of cellular features. Its genetic architecture is heterogeneous, and synaptic mechanisms are implicated alongside monoaminergic signaling.[16] Protocols for producing serotonergic neurons from human pluripotent cells have enabled direct study of treatment-resistant cellular phenotypes.[40] Neurons from patients resistant to selective serotonin reuptake inhibitors display exaggerated serotonin-evoked activity and altered serotonergic arborization, with protocadherin regulation contributing to circuit organization.[11,41,42] Patient-derived cortical neurons have also yielded candidate predictors of antidepressant response.[2] These findings argue against treating MDD as a uniform reduction in neuronal activity; a model should allow one outcome to be elevated while

other functions remain impaired.

Rapid antidepressant actions provide a further reason to analyze trajectories. Ketamine increases structural plasticity in human iPSC-derived dopaminergic neurons through AMPA-receptor, brain-derived neurotrophic factor, and mTOR signaling.[9] A ketamine metabolite can promote dendritic growth on a time scale compatible with clinical exposure.[12] A 6-h response, a 24-h maximum, and a 72-h persistence phase are biologically different events. Collapsing them into one endpoint obscures whether an intervention acts quickly but transiently, slowly but durably, or only after the challenge has begun to resolve spontaneously. Temporal encoding can retain those distinctions in a compact donor-level representation.

BD models emphasize calcium signaling, neuronal excitability, structural plasticity, and inflammatory support from astrocytes. iPSCs from affected families show transcriptional changes in neuronal differentiation and signaling,[22,27] including altered transcripts related to calcium handling and telencephalic fate.[10] Patient-derived neurons separate into subpopulations whose intrinsic activity is associated with clinical lithium responsiveness.[35] Lithium-sensitive pathways include a phosphoregulatory set point involving collapsin response mediator protein-2, which participates in cytoskeletal dynamics.[39] Dysregulation of miR-34a connects neuronal development with genetic risk and reduces synaptic maturation,[3] while mood stabilizers regulate several microRNAs relevant to neuronal protection.[19] Astrocytes derived from BD donors can provide weaker neuronal support and a stronger inflammatory response.[43] These observations justify combining electrical, structural, metabolic, and inflammatory outcomes when judging recovery.

A transdiagnostic view does not erase diagnosis; it tests which biological processes cross the categories and which remain treatment-selective. Reviews of transdiagnostic psychiatry emphasize the value of mechanisms that recur across conventional labels while preserving clinically important heterogeneity.[13,17] Organoids are well suited to this question because the same controlled challenge and measurement schedule can be applied to cells representing different diagnoses. At the same time, precision claims require restraint. Organoid-guided treatment selection remains a developing goal, and model predictions need prospective validation against donor phenotype, technical replication, and ultimately clinical response.[6] A simulation is useful at this stage when it is treated as a design test rather than a substitute for patient material.

The present study asks a focused question: under a shared TNF-α challenge, do multivariate temporal response shapes contain enough information to distinguish virtual donor groups and to rank loxapine, ketamine, and lithium according to broad cellular recovery? A mini-review of psychiatric organoid biology delineated the relevant disease processes and drug-response directions;[44] it is cited here once to acknowledge that conceptual synthesis. The current work differs in purpose and evidence type. It conducts a prespecified factorial simulation, produces donor-level longitudinal records, introduces trajectory-encoded perturbation phenotyping, adds a multireadout recovery calculation and grouped classification, and evaluates sensitivity to the omission of each readout family. The primary expectation was that diagnosis would remain only partly separable because the disorders share biological processes. The second expectation was that drug ranking would become clearer when the complete recovery profile was considered: loxapine for schizophrenia, ketamine for MDD, and lithium for BD. Both expectations are directly testable in the generated dataset and can be challenged later in a donor-blocked wet-laboratory study.

2. MATERIALS AND METHODS

The simulation represents a preclinical experiment in which cortical organoids from 120 virtual donors are exposed to a common inflammatory perturbation and then observed during pharmacological recovery. Four groups contained 30 donors each: unaffected control, schizophrenia, MDD, and BD. The donor, not the well, was the inferential unit. Every donor contributed three organoid replicates to five exposure arms at four times. The exposure arms were unchallenged culture, TNF-α alone, TNF-α plus loxapine, TNF-α plus ketamine, and TNF-α plus lithium. Measurements were recorded at 0, 6, 24, and 72 h. This arrangement yielded $120 \times 5 \times 4 \times 3 = 7{,}200$ organoid records. Five outcomes per record produced 36,000 numerical values.

The intended physical context is shown in figure 1. The images depict plate handling, perfused culture, and automated optical recording as photorealistic methodological visualizations; they are not observations from the simulation and are not presented as microscopy. This distinction is important because a realistic image can clarify the planned assay environment without being used as evidence for a numerical claim.

The design in table 1 separates biological and technical replication. Donor-specific offsets affect all records from one donor, sensitivity to TNF-α varies by donor, and pharmacodynamic responsiveness varies separately for each drug. Triplicate organoids provide technical averaging but do not inflate the donor count. The four observation times were chosen to represent pretreatment state, early response, maximum injury, and late recovery. No clinical outcomes are simulated, and no diagnostic or treatment claim extends beyond the generated conditions.

2.1. Virtual donor generation

Pretreatment group means were specified for the five outcomes using plausible directions from patient-derived neural and organoid studies. Control donors had the highest average network synchrony and mitochon-

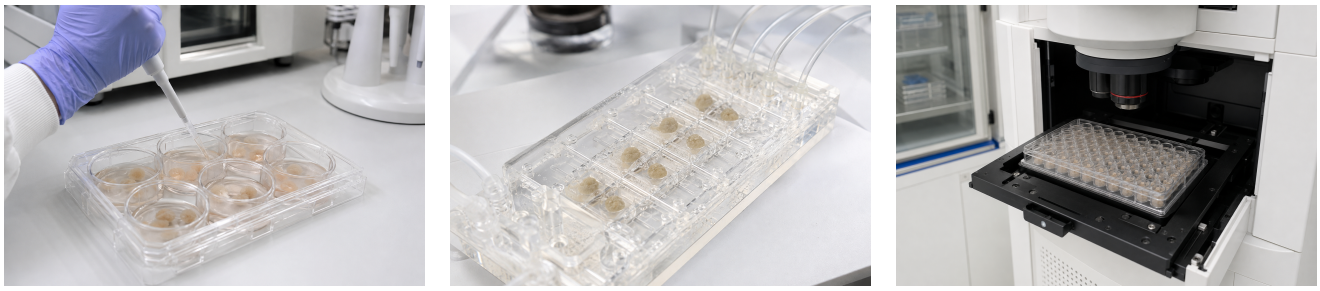

(a) Plate culture **(b)** Perfused chamber **(c)** Automated imaging

Figure 1. Intended assay setting.

Table 1. Factorial study design.

Component	Specification
Virtual donors	120 total; 30 control, 30 schizophrenia, 30 MDD, and 30 BD
Exposure arms	Unchallenged; TNF-α; TNF-α+loxapine; TNF-α+ketamine; TNF-α+lithium
Times	0, 6, 24, and 72 h
Technical replication	Three organoids per donor–exposure–time combination
Cellular outcomes	Network synchrony, neurite complexity, mitochondrial potential, excitation–inhibition balance, and IL-6
Inferential unit	Donor; replicate values averaged before trajectory analysis
Primary analysis	Interval changes and late curvature followed by grouped cross-validation
Secondary analysis	Integrated recovery fraction, donor bootstrap intervals, drug selection, and readout-family omission

drial potential. Schizophrenia donors had lower synchrony, neurite complexity, mitochondrial potential, and excitation–inhibition balance, with modestly increased IL-6. The MDD group retained intermediate synchrony and mitochondrial potential but had increased neurite complexity to represent a treatment-resistant serotonergic branching phenotype rather than a uniform loss of structure. The BD group had reduced synchrony and excitation–inhibition balance and the highest pretreatment IL-6. These settings deliberately create overlap among disorders.

For donor i, group g, outcome k, exposure d, time t, and replicate r, the generated observation was

$$Y_{igkdtr} = \mu_{gk} + b_{ik} + s_i C_{gk} q_t - p_{id} R_{gdk} q_t u_t + \varepsilon_{igkdtr}, \quad (1)$$

where μ_{gk} is the pretreatment group mean, b_{ik} is a donor-specific offset, s_i is donor sensitivity to TNF-α, C_{gk} is the maximum group-specific challenge effect, and q_t governs the challenge time course. The term containing R_{gdk} is included only for a drug exposure; p_{id} is donor-specific pharmacodynamic responsiveness and u_t is the treatment time course. Replicate noise is ε_{igkdtr}. Donor sensitivities were sampled from a truncated normal distribution with mean 1.00 and standard deviation 0.13, bounded at 0.68 and 1.36. Drug responsiveness had mean 1.00 and standard deviation 0.12, bounded at 0.67 and 1.32.

The challenge time coefficients were 0.00, 0.46, 1.00, and 0.72 at 0, 6, 24, and 72 h. Treatment coefficients were 0.00, 0.18, 0.68, and 1.00 at the same times. The challenge therefore reached its greatest magnitude at 24 h and partly resolved by 72 h, whereas treatment action accumulated through the observation period. The equation creates a biologically interpretable competition between injury and recovery. It does not assert that all cellular responses obey a linear pharmacodynamic law; its role is to generate a transparent test bed in which the analysis must recover known but noisy structure.

2.2. Outcome scales and pharmacological recovery

Network synchrony was bounded from 0.05 to 0.98. Neurite complexity was expressed as a Sholl-like intersection count and constrained to remain positive. Mitochondrial membrane potential was expressed in arbitrary units. Excitation–inhibition balance was a dimensionless normalized ratio, and IL-6 was expressed in pg mL^{-1}. Challenge effects were negative for the first four outcomes and positive for IL-6. The greatest TNF-α sensitivity was assigned to schizophrenia and BD, consistent with a design intended to examine developmental neuroimmune vulnerability.

Drug effects were multivariate rather than unrestricted improvements. Loxapine reversed a larger share of the schizophrenia challenge effect, particularly for syn-

chrony, neurite complexity, and excitation–inhibition balance. Ketamine acted most strongly in MDD, with its largest fraction on neurite complexity and synchrony. Lithium acted most strongly in BD, with broad effects on synchrony, mitochondrial potential, excitation–inhibition balance, and IL-6. Each drug also produced smaller responses in the other groups. This overlap prevents the drug-selection analysis from relying on a binary on–off rule.

2.3. Trajectory-encoded perturbation phenotyping

Triplicate organoid values were averaged within each donor, exposure, and time before feature construction. The primary analysis used only the TNF-α-alone arm so that diagnosis prediction could not exploit the name or expected selectivity of a drug. For each donor and outcome, three consecutive changes were calculated: 0–6 h, 6–24 h, and 24–72 h. A late curvature term captured departure from a simple linear return:

$$\kappa_{ik} = Y_{ik,72} - 2Y_{ik,24} + Y_{ik,6}. \tag{2}$$

The resulting donor representation contained 20 features: three interval changes and one curvature value for each of five outcomes. Positive curvature has different raw meaning across outcomes, so all features were standardized within each training fold. The representation preserves response shape while avoiding direct use of the pretreatment group means. Consequently, successful classification must depend on how a donor reacts to the common perturbation, not simply on its starting value.

2.4. Integrated recovery fraction

Drug recovery was calculated within donor and outcome relative to the unchallenged and TNF-α-alone arms. For an outcome in which higher values indicate improvement, the recovery fraction at time t was

$$r_{ikdt} = \frac{Y_{ikdt} - Y_{ik,\mathrm{TNF},t}}{|Y_{ik,\mathrm{unch},t} - Y_{ik,\mathrm{TNF},t}| + 10^{-9}}. \tag{3}$$

For IL-6, the numerator was reversed because lower secretion indicates recovery. Values were limited to the interval $[-0.5, 1.3]$ to prevent a small denominator from dominating a donor profile. Time-specific fractions were combined with weights 0.20, 0.35, and 0.45 at 6, 24, and 72 h. The five outcome-specific fractions were then averaged with equal weight. A value of zero means no improvement relative to TNF-α alone, a value near one means return toward the unchallenged state, and a negative value indicates worsening. Equal weighting was chosen because the simulation does not contain clinical evidence that would justify privileging one cellular outcome.

2.5. Classification, uncertainty, and sensitivity analyses

A multinomial logistic regression with L2 regularization classified the four groups from standardized trajectory features. Five-fold stratified grouped cross-validation kept every record from a donor within one fold. Because the analysis table already contained one row per donor, grouping also served as an explicit guard against any later addition of clone-level rows crossing folds. Accuracy, balanced accuracy, and one-versus-rest F1 were calculated from held-out predictions. An exact binomial test compared the number of correct classifications with chance assignment among four classes.

Uncertainty for mean integrated recovery fractions was estimated by 4,000 donor-level bootstrap resamples within each group and drug. The preferred drug for a virtual donor was the treatment with the largest integrated recovery fraction. Selection accuracy was the proportion of schizophrenia donors assigned loxapine, MDD donors assigned ketamine, and BD donors assigned lithium. These labels reflect the simulated pharmacology and are not clinical prescribing rules.

Sensitivity to readout composition was tested by repeating grouped cross-validation after omitting all synchrony, neurite, mitochondrial, excitation–inhibition, or IL-6 trajectory features in turn. An increase after omission was interpreted as redundancy or noise under the chosen regularization, whereas a decrease indicated that the omitted family contributed information not fully carried by the remaining outcomes. All calculations used Python with NumPy, pandas, SciPy, and scikit-learn. Random generation used seed 41726. The complete script and generated comma-separated files accompany the manuscript.

3. RESULTS AND DISCUSSION

3.1. Pretreatment states overlapped across diagnoses

The generated cohort retained the intended group differences without making diagnosis visually deterministic. Mean pretreatment synchrony was 0.724 in controls, 0.502 in schizophrenia, 0.605 in MDD, and 0.522 in BD. Mitochondrial potential averaged 98.89, 79.25, 88.20, and 85.70 arbitrary units, respectively. IL-6 showed the opposite ordering, with means of 12.31, 18.60, 15.18, and 25.37 pg mL^{-1}. Neurite complexity was highest in MDD at 37.33 intersections and lowest in schizophrenia at 24.88. The full values appear in table 2.

These values should be interpreted as parameters realized with donor and replicate variation, not estimates of population means. Their role is to establish a difficult but structured classification problem. Schizophrenia and BD are close in synchrony, while MDD overlaps both controls and affected groups in mitochondrial potential and IL-6. The elevated MDD neurite count prevents a simplistic assumption that every disorder is characterized by less of every favorable property. This heterogeneity is consistent with treatment-resistant serotonergic models in which excessive branching coexists with altered circuit function. The table therefore documents the bi-

Table 2. Pretreatment cellular states.

Group	Synchrony	Neurite count	Mitochondrial potential	E–I balance	IL-6 (pg mL^{-1})
Control	0.724	34.50	98.89	1.016	12.31
Schizophrenia	0.502	24.88	79.25	0.717	18.60
Major depression	0.605	37.33	88.20	0.920	15.18
Bipolar disorder	0.522	27.37	85.70	0.818	25.37

ological logic of the simulation and also explains why static multivariate classification would not answer the study's temporal question.

The distributions in figure 2 show donor-level overlap more clearly than the means alone. Schizophrenia synchrony is separated from controls but overlaps BD; MDD lies between those groups. Mitochondrial potential preserves an ordered tendency while leaving shared ranges. IL-6 distinguishes BD most strongly but does not isolate schizophrenia from MDD. The visible overlap is desirable because an unrealistically clean partition would inflate downstream accuracy and conceal the value of the perturbation response.

The biological implication is not that these exact values should occur in patient material. Rather, a future experiment should anticipate overlapping distributions and should avoid choosing inclusion thresholds after viewing treatment effects. Donor blocking, clone balance, culture-age control, and blind image analysis would be essential. The simulation also indicates that pretreatment IL-6 may be a useful stratification variable in BD, but it cannot be assumed to represent disease specificity because inflammatory phenotypes occur across diagnoses and cell types.

3.2. TNF-α exposed latent differences in recovery shape

The shared perturbation produced its largest reduction in network synchrony at 24 h and a partial spontaneous return at 72 h. In controls, mean synchrony under TNF-α declined from approximately 0.724 at 0 h to 0.622 at 24 h and returned to 0.653 at 72 h. The corresponding 24-h troughs were approximately 0.310 in schizophrenia, 0.464 in MDD, and 0.318 in BD. Thus, schizophrenia and BD reached similar absolute troughs despite distinct pretreatment inflammatory and metabolic states. This is precisely the type of convergence that can make a single endpoint ambiguous.

Drug-specific trajectories in figure 3 separated more clearly during late recovery. Loxapine increased schizophrenia synchrony to about 0.477 at 72 h, whereas ketamine and lithium reached about 0.425 and 0.421. Ketamine produced the largest MDD return, reaching approximately 0.584, compared with values near 0.543–0.545 under loxapine and lithium. Lithium produced the largest BD recovery, reaching approximately 0.495, while loxapine and ketamine remained near 0.433–0.440. In controls, all three drugs produced smaller and more similar changes.

The temporal profiles clarify two points that an endpoint comparison would conceal. First, the most effective drug did not prevent the early 6-h decline because treatment action was specified to accumulate gradually. A 6-h assay alone would therefore underestimate selective recovery. Second, TNF-α injury had already begun to resolve at 72 h. A drug-versus-pretreatment comparison would mix pharmacological rescue with spontaneous return, whereas the within-time comparison against TNF-α alone separates those components. A laboratory study should retain the unchallenged and challenge-only arms at every time rather than using a single common control.

The schizophrenia response accords with evidence that antipsychotic action may improve connectivity and developmental signaling without normalizing every cellular abnormality. The MDD response reflects the rapid structural-plasticity literature surrounding ketamine, but the model avoids equating more branching with universal improvement; synchrony, mitochondrial potential, excitation–inhibition balance, and IL-6 must also contribute. The BD response captures a slower, broader lithium effect consistent with altered excitability and cytoskeletal regulation. These interpretations concern alignment between simulation rules and published biology, not confirmation of a causal pathway.

3.3. Multireadout recovery produced disorder-selective drug ranking

The integrated recovery calculation yielded a clear drug ordering within each disorder while retaining between-donor variation. For schizophrenia, loxapine achieved a mean fraction of 0.506 (95% bootstrap interval 0.467–0.547), compared with 0.280 for ketamine and 0.295 for lithium. For MDD, ketamine reached 0.499 (0.471–0.528), compared with 0.218 for loxapine and 0.282 for lithium. For BD, lithium reached 0.571 (0.538–0.604), compared with 0.248 for loxapine and 0.300 for ketamine. These values are listed in table 3.

The magnitude of recovery is intentionally below complete restoration. Even the best disorder–drug pairing returned only about one-half of the multivariate distance between challenge and unchallenged culture. This restraint matters for interpretation. A strong change in one pathway does not imply normalization of a complex disorder phenotype, and complete recovery would be im-

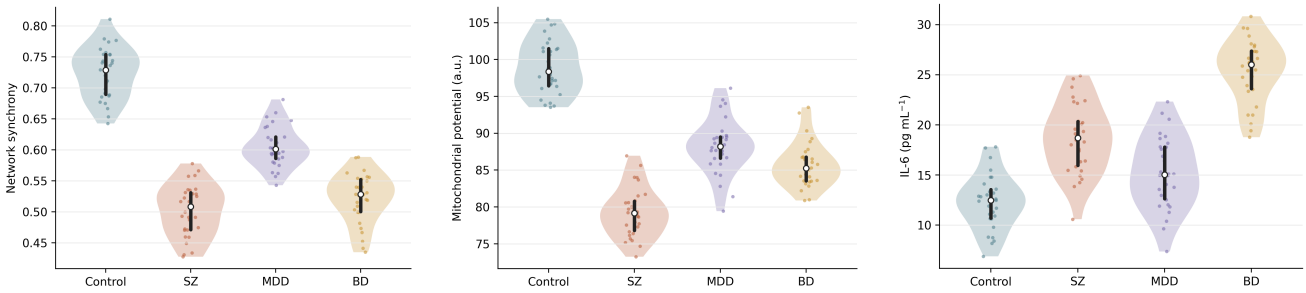

(a) Synchrony **(b)** Mitochondria **(c)** IL-6

Figure 2. Pretreatment donor distributions.

Table 3. Integrated pharmacological recovery.

Group	Drug	Mean recovery	95% bootstrap interval
Schizophrenia	Loxapine	0.506	0.467–0.547
	Ketamine	0.280	0.252–0.306
	Lithium	0.295	0.274–0.316
Major depression	Loxapine	0.218	0.188–0.247
	Ketamine	0.499	0.471–0.528
	Lithium	0.282	0.245–0.318
Bipolar disorder	Loxapine	0.248	0.223–0.273
	Ketamine	0.300	0.272–0.326
	Lithium	0.571	0.538–0.604

plausible under a short exposure in developing tissue. The bootstrap intervals quantify uncertainty among virtual donors, but they do not include uncertainty about the biological assumptions used to set the generating parameters.

The readout-specific profiles in figure 4 explain why the integrated values differ. Loxapine's schizophrenia advantage was broad, with the largest gains in synchrony, neurites, and excitation–inhibition balance. Ketamine's MDD advantage was concentrated in neurite complexity and synchrony, with more moderate improvement in mitochondrial potential and IL-6. Lithium's BD advantage covered synchrony, mitochondrial potential, excitation–inhibition balance, and IL-6. Because the five outcomes were weighted equally, a drug could not win by producing one extreme response while leaving the other four near the challenge-only state.

Donor-level drug selection was correct under the generating rules for all 30 schizophrenia donors, 28 of 30 MDD donors, and all 30 BD donors. The two MDD mismatches occurred because donor-specific ketamine responsiveness was low while lithium responsiveness was high. This outcome demonstrates an important difference between group ranking and individual assignment. A clear group mean does not guarantee uniform donor behavior. In real patient-derived cultures, selection accuracy would probably be lower because clone variation, differentiation quality, medication history, polypharmacy, and unmodeled cell types would add uncertainty. The present calculation is best understood as a power and analysis-design test.

Equal weighting also deserves scrutiny. Network synchrony and excitation–inhibition balance are related electrical properties, while IL-6 and mitochondrial potential may respond on different time scales. Equal weighting protects against unverified clinical priorities but may count correlated evidence twice. A wet-laboratory study could prespecify a primary outcome, retain the remaining measurements as secondary, and use a hierarchical model to estimate a shared recovery component without erasing outcome-specific effects. Such a choice should be made before treatment labels are revealed.

3.4. Trajectory features achieved partial out-of-donor separation

The first two principal axes of the standardized trajectory representation accounted for 46.6% and 10.2% of its variance. The donor projection in figure 5a separated controls from most affected donors along the first axis, while schizophrenia, MDD, and BD retained considerable overlap. This geometry is compatible with the study premise: shared neuroimmune injury creates a common direction of change, whereas diagnosis modifies the magnitude and curvature of that change.

Five-fold grouped cross-validation classified 84 of 120

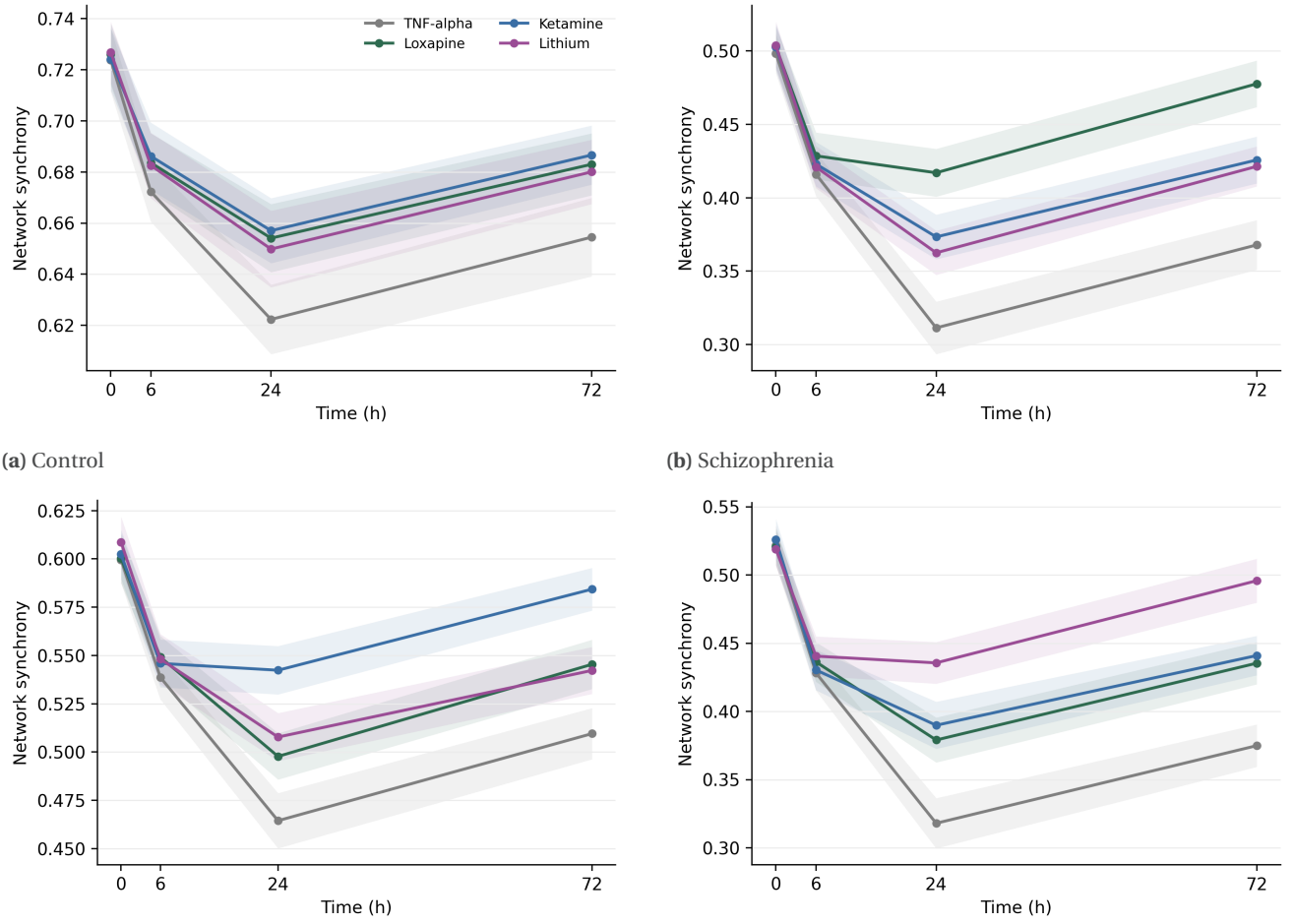

(a) Control

(b) Schizophrenia

(c) Major depression

(d) Bipolar disorder

Figure 3. Network synchrony through 72 hours.

donors correctly, giving accuracy and balanced accuracy of 0.700. The exact binomial comparison with four-class chance assignment gave $p = 5.36 \times 10^{-25}$. F1 was 0.900 for controls, 0.585 for schizophrenia, 0.632 for MDD, and 0.690 for BD. The class-wise values are shown in figure 5b. The lower schizophrenia and MDD values are consistent with the overlap visible in the projection. High control performance reflects its milder TNF-α response rather than simple pretreatment differences, because only interval changes and curvature from the challenge arm entered classification.

Partial separation is more credible than near-perfect prediction in this setting. The three disorders share synaptic, metabolic, and inflammatory processes, and a single cytokine challenge cannot be expected to expose every disease-specific mechanism. The result suggests that dynamic response contributes information, but it also sets an upper bound under favorable conditions. A future laboratory test should compare the trajectory classifier with models using pretreatment values alone, 24-h values alone, and 72-h values alone. Improvement must be evaluated on donors withheld from every stage of normalization and feature selection.

Logistic regression was chosen for interpretability and to limit overfitting with 120 donors. More flexible algorithms could raise apparent accuracy, particularly in a deterministic simulation, but would require nested tuning and a larger cohort. The present feature count of 20 is already substantial relative to 120 donors. Regularization, grouped folds, and a fixed seed make the result auditable, yet confidence intervals across several independently generated cohorts would be needed to characterize simulation-to-simulation variation.

3.5. Readout omission revealed information and redundancy

The sensitivity analysis in table 4 showed that removing IL-6 features produced the largest loss, reducing balanced accuracy from 0.700 to 0.650. Removing mitochondrial features yielded 0.692, close to the full model. By contrast, removal of neurite features increased balanced accuracy to 0.733, and removal of excitation–inhibition features increased it to 0.758. Removing synchrony left the value unchanged at 0.700.

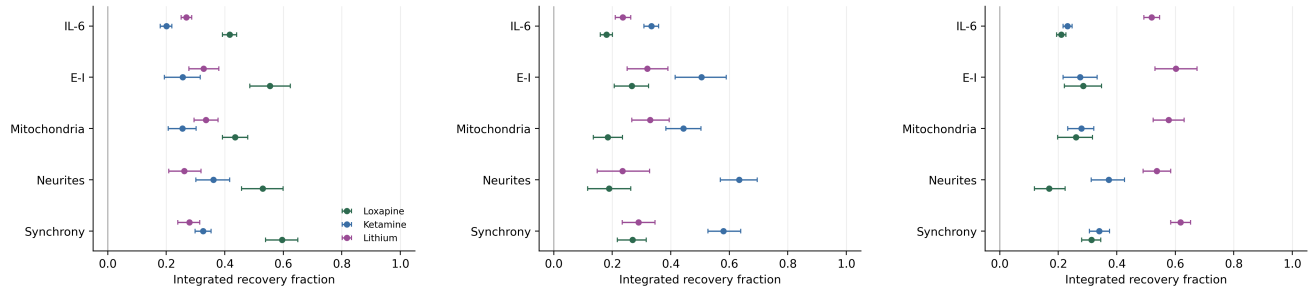

(a) Schizophrenia **(b)** Major depression **(c)** Bipolar disorder

Figure 4. Recovery profiles across five cellular readouts.

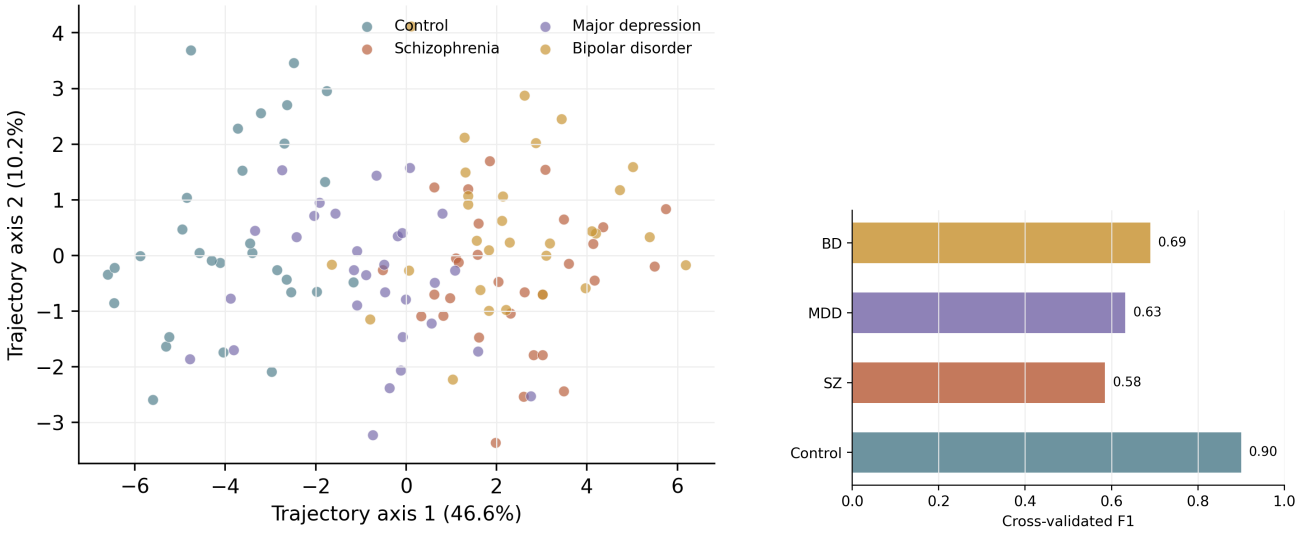

(a) Trajectory projection **(b)** Held-out F1

Figure 5. Donor-level trajectory classification.

Table 4. Readout-family omission.

Omitted family	Balanced accuracy
None	0.700
Synchrony	0.700
Neurites	0.733
Mitochondria	0.692
Excitation–inhibition	0.758
IL-6	0.650

The IL-6 result follows from the deliberately different inflammatory amplitudes, especially the high BD response. It does not mean that IL-6 is a diagnostic biomarker. In a real assay, secreted cytokine values are sensitive to organoid size, medium volume, cell composition, and sampling interval. Normalization to viable cell mass and careful accounting for repeated medium exchange would be required. The analysis instead shows that an inflammatory trajectory can add information when measured consistently with electrical and metabolic outcomes.

Accuracy gains after omitting neurite or excitation–inhibition features indicate redundancy and finite-sample noise. Synchrony and excitation–inhibition balance share part of the same generated injury pattern; retaining both can destabilize a linear boundary. Neurite change also responds strongly to ketamine-like rules that were not used in the challenge-only classifier, leaving less diagnosis-specific information than its biological importance might suggest. This distinction matters: a readout can be valuable for pharmacological interpretation even if it does not improve diagnostic classification.

The omission analysis therefore discourages indiscriminate assay expansion. Adding more channels does not guarantee better donor prediction. Measurements should be selected for distinct biological content, technical reliability, and relevance to the prespecified question. A practical wet-laboratory panel might retain one electrical feature, one structural feature, one metabolic feature, and one secreted inflammatory feature, then test whether a second electrical outcome adds independent value.

3.6. Implications for organoid pharmacology

The principal result is methodological: response shape can be treated as a donor phenotype. A cell model is often described by what it is before treatment, but its capacity to absorb injury and return toward a stable state may be more informative. Interval changes distinguish early susceptibility from late recovery, and curvature distinguishes monotonic decline from rebound. This view is compatible with psychiatric disorders in which genetic liability interacts with developmental stress and treatment response varies widely among individuals.

The multireadout design also changes the meaning of drug efficacy. Loxapine, ketamine, and lithium act through different proximal targets, yet their desirable cellular consequences can converge on connectivity, plasticity, energy handling, and inflammatory regulation. Measuring these consequences on a common scale permits comparison without claiming that the drugs are interchangeable. The simulation's disorder-selective ordering was built into the generating process, but the analysis recovered it despite donor variation, technical noise, and partial spontaneous resolution. This verifies the internal logic of the planned experiment.

Translation would require several safeguards. Donor recruitment should include medication exposure, episode state, sex, age, ancestry, smoking, and relevant medical conditions because each may influence iPSC-derived phenotypes. At least two independently validated clones per donor and several differentiations per clone would be needed to estimate technical variation. Organoid size and cell composition should be measured before randomization. Drug allocation and image analysis should be concealed from operators. Plate layout should distribute diagnoses and treatments across positions to prevent edge effects from mimicking biology. Concentrations should be selected from pharmacologically plausible free exposures and preceded by toxicity testing.

Temporal sampling presents another challenge because destructive assays cannot be repeated in the same organoid. Electrical recordings and medium sampling can be longitudinal, whereas transcriptomic or histological measurements require matched organoids harvested at each time. The statistical model must distinguish repeated observations from parallel destructive samples. The current simulation treats all five outcomes as repeatable, which is convenient for analysis but biologically optimistic. A laboratory implementation could use continuous electrical recording and secreted IL-6 longitudinally, with neurite and mitochondrial imaging repeated only if phototoxicity is acceptable.

Clinical interpretation must remain separate from cellular ranking. The preferred drug in this dataset is defined by the generating rules and by equal weighting of five outcomes. It does not predict symptom remission, adverse effects, dose requirements, or long-term relapse prevention. A credible precision-psychiatry study would need a locked analysis applied prospectively to donors whose treatment response is unknown during culture. Even then, an organoid result would be one piece of evidence rather than an autonomous prescribing decision.

4. CONCLUSION

This study asked whether temporal responses to a common neuroimmune challenge could distinguish schizophrenia, MDD, and BD donor phenotypes and identify the drug producing the broadest cellular recovery. Within a transparent simulation of 120 virtual donors, the answer was yes, but not perfectly. Interval changes and curvature across five readouts yielded 0.700 balanced accuracy, indicating that response shape carried diagnostic information while preserving substantial overlap among the disorders. The same longitudinal records produced disorder-selective recovery rankings: loxapine for schizophrenia, ketamine for MDD, and lithium for BD. IL-6 contributed the most unique classification information, whereas excitation–inhibition and neurite features were partly redundant under the linear classifier.

The conclusion is therefore specific: temporal multireadout phenotyping can recover a noisy, biologically structured treatment signal that isolated endpoints would incompletely describe. It does not show that organoids can presently choose treatment for patients. The next decisive test is a donor-blocked, blinded organoid experiment using the same exposure arms, observation times, and locked equations, with technical variance estimated across clones and differentiations. Success should require improved held-out prediction over static measurements and concordance between cellular recovery and independently recorded treatment response. Until those conditions are met, the present findings remain a reproducible design study and a set of falsifiable quantitative expectations.

FUNDING

No external funding was received.

CONFLICT OF INTEREST

The author declares no commercial or financial relationship that could be construed as a potential conflict of interest.

BIBLIOGRAFIA / REFERENCES

1. A. I. Abdullah, A. Pollock, and T. Sun, "The path from skin to brain: generation of functional neurons from fibroblasts," *Molecular Neurobiology*, *45*, 586–595, 2012. doi:10.1007/s12035-012-8277-6.
2. Y. Avior, S. Ron, D. Kroitorou, C. Albeldas, V. Lerner, B. Corneo, et al., "Depression patient-derived cortical neurons reveal potential biomarkers for antidepressant response," *Translational Psychiatry*, *11*, 201, 2021. doi:10.1038/s41398-021-01319-5.
3. S. Bavamian, N. Mellios, J. Lalonde, D. M. Fass, J.

Wang, S. D. Sheridan, et al., "Dysregulation of miR-34a links neuronal development to genetic risk factors for bipolar disorder," *Molecular Psychiatry*, *20*, 573–584, 2015. doi:10.1038/mp.2014.176.

4. C. A. Benson, H. R. Powell, M. Liput, S. Dinham, D. A. Freedman, T. A. Ignatowski, et al., "Immune factor TNF-α disrupts human brain organoid development and increases developmental vulnerability in schizophrenia," *Frontiers in Cellular Neuroscience*, *14*, 233, 2020.
5. F. Birey, J. Andersen, C. D. Makinson, S. Islam, W. Wei, N. Huber, et al., "Assembly of functionally integrated human forebrain spheroids," *Nature*, *545*, 54–59, 2017. doi:10.1038/nature22330.
6. S. Bose, H. Clevers, and X. Shen, "Promises and challenges of organoid-guided precision medicine," *Med*, *2*, 1011–1026, 2021. doi:10.1016/j.medj.2021.08.005.
7. K. J. Brennand, A. Simone, J. Jou, C. Gelboin-Burkhart, N. Tran, S. Sangar, et al., "Modelling schizophrenia using human induced pluripotent stem cells," *Nature*, *473*, 221–225, 2011. doi:10.1038/nature09915.
8. K. Brennand, J. N. Savas, Y. Kim, N. Tran, A. Simone, K. Hashimoto-Torii, et al., "Phenotypic differences in hiPSC neural progenitor cells derived from patients with schizophrenia," *Molecular Psychiatry*, *20*, 361–368, 2015. doi:10.1038/mp.2014.22.
9. L. Cavalleri, E. Merlo Pich, M. J. Millan, C. Chiamulera, T. Kunath, P. F. Spano, et al., "Ketamine enhances structural plasticity in mouse mesencephalic and human iPSC-derived dopaminergic neurons via AMPAR-driven BDNF and mTOR signaling," *Molecular Psychiatry*, *23*, 812–823, 2018. doi:10.1038/mp.2017.241.
10. H. M. Chen, C. J. DeLong, M. Bame, I. Rajapakse, T. J. Herron, M. G. McInnis, et al., "Transcripts involved in calcium signaling and telencephalic neuronal fate are altered in induced pluripotent stem cells from bipolar disorder patients," *Translational Psychiatry*, *4*, e375, 2014. doi:10.1038/tp.2014.12.
11. W. V. Chen, C. L. Nwakeze, C. A. Denny, S. O'Keeffe, M. A. Rieger, G. Mountoufaris, et al., "Pcdhαc2 is required for axonal tiling and assembly of serotonergic circuitries in mice," *Science*, *356*, 406–411, 2017. doi:10.1126/science.aal3231.
12. G. Collo, L. Cavalleri, C. Chiamulera, and E. M. Pich, "(2R,6R)-hydroxynorketamine promotes dendrite outgrowth in human inducible pluripotent stem cell-derived neurons through AMPA receptor signaling," *NeuroReport*, *29*, 1425–1430, 2018. doi:10.1097/WNR.0000000000001131.
13. T. Dalgleish, M. Black, D. Johnston, and A. Bevan, "Transdiagnostic approaches to mental health problems: current status and future directions," *Journal of Consulting and Clinical Psychology*, *88*, 179–195, 2020. doi:10.1037/ccp0000482.
14. K. Duval, H. Grover, L. H. Han, Y. Mou, A. F. Pegoraro, J. J. Fredberg, et al., "Modeling physiological events in 2D versus 3D cell culture," *Physiology*, *32*, 266–277, 2017. doi:10.1152/physiol.00036.2016.
15. N. Eura, T. K. Matsui, J. Luginbühl, M. Matsubayashi, H. Nanaura, T. Shiota, et al., "Brainstem organoids from human pluripotent stem cells," *Frontiers in Neuroscience*, *14*, 538, 2020. doi:10.3389/fnins.2020.00538.
16. J. Flint and K. S. Kendler, "The genetics of major depression," *Neuron*, *81*, 1214, 2014. doi:10.1016/j.neuron.2014.02.033.
17. P. Fusar-Poli, M. Solmi, N. Brondino, C. Davies, C. Chae, P. Politi, et al., "Transdiagnostic psychiatry: a systematic review," *World Psychiatry*, *18*, 192–207, 2019. doi:10.1002/wps.20631.
18. K. Hashimoto-Torii, M. Torii, M. Fujimoto, A. Nakai, R. El Fatimy, V. Mezger, et al., "Roles of heat shock factor 1 in neuronal response to fetal environmental risks and its relevance to brain disorders," *Neuron*, *82*, 560–572, 2014. doi:10.1016/j.neuron.2014.03.002.
19. J. G. Hunsberger, E. B. Fessler, F. L. Chibane, Y. Leng, and D. Maric, "Mood stabilizer-regulated miRNAs in neuropsychiatric and neurodegenerative diseases," *American Journal of Translational Research*, *5*, 450–464, 2013.
20. D. E. Ingber, "Human organs-on-chips for disease modelling, drug development and personalized medicine," *Nature Reviews Genetics*, *23*, 467–491, 2022. doi:10.1038/s41576-022-00466-9.
21. J. Jo, Y. Xiao, A. X. Sun, E. Cukuroglu, H. D. Tran, J. Göke, et al., "Midbrain-like organoids from human pluripotent stem cells contain functional dopaminergic and neuromelanin-producing neurons," *Cell Stem Cell*, *19*, 248–257, 2016. doi:10.1016/j.stem.2016.07.005.
22. K. H. Kim, J. Liu, R. J. S. Galvin, J. L. Dage, J. A. Egeland, R. C. Smith, et al., "Transcriptomic analysis of induced pluripotent stem cells derived from patients with bipolar disorder from an Old Order Amish pedigree," *PLoS ONE*, *10*, e0142693, 2015. doi:10.1371/journal.pone.0142693.
23. E. Knight and S. Przyborski, "Advances in 3D cell culture technologies enabling tissue-like structures to be created in vitro," *Journal of Anatomy*, *227*, 746–756, 2015. doi:10.1111/joa.12257.
24. G. Konopka, T. Friedrich, J. Davis-Turak, K. Winden, M. C. Oldham, F. Gao, et al., "Human-specific transcriptional networks in the brain," *Neuron*, *75*, 601–617, 2012. doi:10.1016/j.neuron.2012.05.034.
25. G. La Manno, D. Gyllborg, S. Codeluppi, K. Nishimura, C. Salto, A. Zeisel, et al., "Molecular diversity of midbrain development in mouse, human, and stem cells," *Cell*, *167*, 566–580.e19, 2016. doi:10.1016/j.cell.2016.09.027.
26. M. A. Lancaster, M. Renner, C. A. Martin, D. Wenzel, L. S. Bicknell, M. E. Hurles, et al., "Cerebral organoids model human brain development and microcephaly," *Nature*, *501*, 373–379, 2013. doi:10.1038/nature12517.
27. J. M. Madison, F. Zhou, A. Nigam, A. Hussain, D. D. Barker, R. Nehme, et al., "Characterization of bipolar disorder patient-specific induced pluripotent stem cells from a family reveals neurodevelopmental and

mRNA expression abnormalities," *Molecular Psychiatry*, *20*, 703–717, 2015. doi:10.1038/mp.2015.7.

28. K. Muguruma, A. Nishiyama, H. Kawakami, K. Hashimoto, and Y. Sasai, "Self-organization of polarized cerebellar tissue in 3D culture of human pluripotent stem cells," *Cell Reports*, *10*, 537–550, 2015. doi:10.1016/j.celrep.2014.12.051.
29. S. T. Narla, Y. W. Lee, C. A. Benson, P. Sarder, K. J. Brennand, E. K. Stachowiak, et al., "Common developmental genome deprogramming in schizophrenia: role of integrative nuclear FGFR1 signaling," *Schizophrenia Research*, *185*, 17–32, 2017. doi:10.1016/j.schres.2016.12.012.
30. T. Ogura, H. Sakaguchi, S. Miyamoto, and J. Takahashi, "Three-dimensional induction of dorsal, intermediate and ventral spinal cord tissues from human pluripotent stem cells," *Development*, *145*, dev162214, 2018. doi:10.1242/dev.162214.
31. X. Qian, Y. Su, C. D. Adam, A. U. Deutschmann, S. R. Pather, E. M. Goldberg, et al., "Sliced human cortical organoids for modeling distinct cortical layer formation," *Cell Stem Cell*, *26*, 766–781.e9, 2020. doi:10.1016/j.stem.2020.02.002.
32. O. Robicsek, R. Karry, I. Petit, N. Salman-Kesner, F. J. Müller, E. Klein, et al., "Abnormal neuronal differentiation and mitochondrial dysfunction in hair follicle-derived induced pluripotent stem cells of schizophrenia patients," *Molecular Psychiatry*, *18*, 1067–1076, 2013. doi:10.1038/mp.2013.67.
33. O. Robicsek, H. M. Ene, R. Karry, O. Ytzhaki, E. Asor, D. McPhie, et al., "Isolated mitochondria transfer improves neuronal differentiation of schizophrenia-derived induced pluripotent stem cells and rescues deficits in a rat model," *Schizophrenia Bulletin*, *44*, 432–442, 2018. doi:10.1093/schbul/sbx077.
34. T. Sawada, T. E. Chater, Y. Sasagawa, M. Yoshimura, N. Fujimori-Tonou, K. Tanaka, et al., "Developmental excitation–inhibition imbalance underlying psychoses revealed by single-cell analyses of discordant twin-derived cerebral organoids," *Molecular Psychiatry*, *25*, 2695–2711, 2020. doi:10.1038/s41380-020-0844-z.
35. S. Stern, R. Santos, M. C. Marchetto, A. P. D. Mendes, G. A. Rouleau, S. Biesmans, et al., "Neurons derived from patients with bipolar disorder divide into intrinsically different sub-populations predicting responsiveness to lithium," *Molecular Psychiatry*, *23*, 1453–1465, 2018. doi:10.1038/mp.2016.260.
36. E. K. Stachowiak, C. A. Benson, S. T. Narla, A. Dimitri, L. E. B. Chuye, S. Dhiman, et al., "Cerebral organoids reveal early cortical maldevelopment in schizophrenia: computational anatomy and genomics, role of FGFR1," *Translational Psychiatry*, *7*, 6, 2017. doi:10.1038/s41398-017-0054-x.
37. H. Tabata, S. Yoshinaga, and K. Nakajima, "Cytoarchitecture of mouse and human subventricular zone in developing cerebral neocortex," *Experimental Brain Research*, *216*, 161–168, 2012. doi:10.1007/s00221-011-2933-3.
38. K. Takahashi and S. Yamanaka, "Induction of pluripotent stem cells from mouse embryonic and adult fibroblast cultures by defined factors," *Cell*, *126*, 663–676, 2006. doi:10.1016/j.cell.2006.07.024.
39. B. T. D. Tobe, A. M. Crain, A. M. Winquist, B. Calabrese, H. Makihara, W. N. Zhao, et al., "Probing the lithium-response pathway in hiPSCs implicates the phosphoregulatory set point for a cytoskeletal modulator in bipolar pathogenesis," *Proceedings of the National Academy of Sciences USA*, *114*, E4462–E4471, 2017. doi:10.1073/pnas.1700111114.
40. K. C. Vadodaria, M. C. Marchetto, J. Mertens, and F. H. Gage, "Generating human serotonergic neurons in vitro: methodological advances," *BioEssays*, *38*, 1123–1129, 2016. doi:10.1002/bies.201600127.
41. K. C. Vadodaria, Y. Ji, M. Skime, A. Paquola, T. Nelson, D. Hall-Flavin, et al., "Serotonin-induced hyperactivity in SSRI-resistant major depressive disorder patient-derived neurons," *Molecular Psychiatry*, *24*, 795–807, 2019. doi:10.1038/s41380-019-0363-y.
42. K. C. Vadodaria, Y. Ji, M. Skime, A. C. Paquola, T. Nelson, D. Hall-Flavin, et al., "Altered serotonergic circuitry in SSRI-resistant major depressive disorder patient-derived neurons," *Molecular Psychiatry*, *24*, 808–818, 2019. doi:10.1038/s41380-019-0377-5.
43. K. C. Vadodaria, A. P. D. Mendes, A. Mei, V. Racha, G. Erikson, M. N. Shokhirev, et al., "Altered neuronal support and inflammatory response in bipolar disorder patient-derived astrocytes," *Stem Cell Reports*, *16*, 825–835, 2021. doi:10.1016/j.stemcr.2021.02.004.
44. R. Villanueva, "Advances in the knowledge and therapeutics of schizophrenia, major depression disorder, and bipolar disorder from human brain organoid research," *Frontiers in Psychiatry*, *14*, 1178494, 2023. doi:10.3389/fpsyt.2023.1178494.
45. Y. S. Zhang, J. Aleman, S. R. Shin, T. Kilic, D. Kim, S. A. Mousavi Shaegh, et al., "Multisensor-integrated organs-on-chips platform for automated and continual in situ monitoring of organoid behaviors," *Proceedings of the National Academy of Sciences USA*, *114*, E2293–E2302, 2017. doi:10.1073/pnas.1612906114.